NASA TECHNICAL NOTE

NASA TN D-5058

NASA TN D-5058

LATERAL SLOSHING IN CYLINDERS UNDER LOW-GRAVITY CONDITIONS

by Jack A. Salzman and William J. Masica

Lewis Research Center
Cleveland, Ohio

NATIONAL AERONAUTICS AND SPACE ADMINISTRATION • WASHINGTON, D. C. • FEBRUARY 1969

NASA TN D-5058

LATERAL SLOSHING IN CYLINDERS UNDER LOW-GRAVITY CONDITIONS

By Jack A. Salzman and William J. Masica

Lewis Research Center
Cleveland, Ohio

NATIONAL AERONAUTICS AND SPACE ADMINISTRATION

For sale by the Clearinghouse for Federal Scientific and Technical Information
Springfield, Virginia 22151 – CFSTI price $3.00

ABSTRACT

An experimental investigation was conducted to determine liquid sloshing characteristics in cylinders with hemispherical bottoms under low Bond number conditions. Static contact angles were restricted to near 0^{o} so that the equilibrium liquid surface was nearly hemispherical at very low Bond numbers. The experiments were conducted in both normal- and low-gravity environments. Data were obtained at Bond numbers ranging from 0 to greater than 800. The natural frequency and damping of the fundamental asymmetric sloshing mode at deep liquid depths were correlated in terms of known system parameters. The natural frequency data at shallow liquid depths were compared with existing theoretical studies. All results were compared with previous normal-gravity experimental sloshing studies.

LATERAL SLOSHING IN CYLINDERS UNDER LOW-GRAVITY CONDITIONS

by Jack A. Salzman and William J. Masica

Lewis Research Center

SUMMARY

As a part of the general study of liquid behavior in low-gravity environments, an experimental investigation was conducted to determine liquid sloshing characteristics under low Bond number conditions. The test tank geometry was a right-circular cylinder with a hemispherical bottom. Static contact angles were restricted to near 0^{o} so that the equilibrium liquid surface was nearly hemispherical at very low Bond numbers. The experiments were conducted in both normal- and low-gravity environments. The low-gravity experiments were conducted in a 5-second free-fall facility. Data were obtained at Bond numbers ranging from 0 ($\approx$0.001) to greater than 800. The natural frequency and damping of the fundamental asymmetric sloshing mode at deep liquid depths were correlated in terms of known system parameters. The natural frequency data at shallow liquid depths were compared with existing theoretical studies. All results were compared with previous normal-gravity experimental sloshing studies.

INTRODUCTION

An understanding of liquid-propellant sloshing is necessary to analyze rocket vehicle control and stability with possible coupled fluid oscillations. Therefore, liquid sloshing has attracted the interest of many investigators. A comprehensive summary of high Bond number sloshing investigations and some of the original work in low Bond number asymmetric or lateral sloshing is contained in reference 1. (Bond number is a dimensionless parameter essentially indicating the ratio of acceleration to capillary forces.) For high Bond numbers (e.g., greater than 100), where the equilibrium liquid surface is reasonably flat, analytical and experimental correlations exist for a wide range of symmetric and asymmetric sloshing phenomena pertinent to space vehicle application. For low Bond numbers, and especially with small contact angles, where the

equilibrium interface is highly curved, only limited information relating to lateral sloshing is available.

One experimental study of lateral sloshing was performed by Clark and Stephens (ref. 2). Their experiments were conducted under normal-gravity (or 1-g) conditions using small-diameter cylinders. Only deep liquid depths ($h/R > 2$) were considered. Empirical relations were obtained that describe the natural frequency and damping at Bond numbers ranging from 8 to about 1000. Another experimental study of low-Bond-number lateral slosh was performed by Dodge and Garza (ref. 3). Their experiments were also conducted at normal gravity. The effects of liquid depth were emphasized. In general, the results of these two studies agree, although the empirical relations for damping differ in form. An experimental study of the sloshing natural frequency and damping in cylinders at zero Bond numbers (≈ 0.001) was performed by the authors (ref. 4). This study was extended (ref. 5) to include the effects of liquid depth for flat-bottom and hemispherical-bottom cylinders. The results of these studies at zero Bond numbers cannot be obtained by extrapolating the relations presented in references 2 and 3.

An analytical study of low Bond number lateral slosh was performed by Concus, Crane, and Satterlee (ref. 6). The tank geometry was a cylinder with a hemispherical bottom. Their linearized inviscid analysis included the effects of contact angle and interface curvature. A finite difference technique was used to compute normal-mode slosh frequency parameters at discrete Bond numbers and liquid depths. Bond numbers ranged from 0 to 50. The results agree with the zero Bond number experimental results presented in references 4 and 5. No comparisons have been made at Bond numbers other than 0.

This report presents the results of an experimental investigation on small-amplitude, lateral (asymmetric) sloshing in cylinders with hemispherical bottoms. The liquids used in the study had static contact angles very near 0° on the cylinders' surfaces. The experiments were conducted in both normal- and low-gravity environments. The low-gravity experiments were conducted in a 5-second free-fall facility. Data were obtained on the natural slosh frequency and damping at Bond numbers ranging from 0 to greater than 800. The sloshing equilibrium liquid surface at these Bond numbers correspondingly ranged from a hemispherical to an essentially flat shape. The effect of liquid depth was included. The natural frequency and damping data for deep liquid depths are presented and correlated in terms of known system parameters. Shallow liquid depth data are presented and compared with existing theoretical studies. The results are also compared with previous normal-gravity experimental sloshing studies (refs. 2 and 3).

SYMBOLS

A	fraction of slosh wave amplitude
A_n	n^{th}-cycle slosh amplitude, cm
A_0	initial slosh amplitude, cm
a	acceleration, cm/sec^2
Bo	Bond number, $Bo = \frac{aR^2}{\beta}$
g	acceleration due to gravity, 981 cm/sec^2
h	centerline interface height from tank bottom, cm
K	nondimensional constant
K_d	nondimensional damping constant or normalized logarithmic decrement
n	cycle number
R	cylinder radius, cm
T	free slosh damping time, sec
t_F	formation time, sec
V	interface edge velocity, cm/sec
α	damping coefficient, sec^{-1}
β	specific surface tension, σ/ρ, cm^3/sec^2
δ	logarithmic decrement, $\delta = \frac{1}{n} \ln \frac{A_0}{A_n}$
η	viscosity, cP
θ_d	dynamic contact angle, deg
θ_s	static contact angle, deg
λ_1	normal-gravity fundamental spherical tank eigenvalue
ρ	liquid density, g/cm^3
σ	surface tension, dynes/cm (or 10^{-5} N/cm)
Ω^2	natural frequency parameter, $\Omega^2 = \frac{\omega_1^2 R^3}{\beta}$
ω_d	damped natural frequency, rad/sec
ω_1	natural frequency, rad/sec

APPARATUS AND PROCEDURE

Lewis Zero-Gravity Facility

The low-gravity data for this study were obtained in the Lewis Zero-Gravity Facility. A schematic of this facility is shown in figure 1. The facility is basically a shaft that extends 155 meters below ground level. The shaft has a concrete liner that is 8.5 meters in diameter. A welded steel vacuum chamber, 6.1 meters in diameter and 142 meters high, is contained inside the concrete liner. A nominal chamber pressure of 13.3 newtons per square meter (1.3×10^{-4} atm) is obtained by using the Lewis wind tunnel exhaust system in series with vacuum pumps located in the facility. Normal pumpdown time is about 1 hour.

The facility has a service building at ground level that contains a shop area, a control room, and a clean room. The control room (fig. 2) contains the controls for establishing the chamber vacuum level, for test operations, and for data retrieval. The clean room, which is used for experiment preparation, is maintained at a Class 10 000 rating. The room contains an ultrasonic cleaner and a Class 100 laminar flow work station for preparing experiments requiring more than normal cleanliness. Instruments to measure fluid properties (such as surface tension, contact angle, etc.) pertinent to low-gravity fluid studies are also included.

The facility has two methods of operation. One method is to allow an experiment vehicle to free-fall from the top of the vacuum chamber. This results in about 5 seconds of free-fall time. The second method is to project the vehicle upwards from the bottom of the chamber by a gas-pressure-operated accelerator. The total up-and-down flight of the experiment vehicle results in about 10 seconds of free-fall time. Both operations use the same recovery system. The experiment vehicle is recovered in a 3.6-meter-diameter, 6.1-meter-deep cart filled with small pellets of expanded polystyrene. The deceleration rate is controlled by the flow of pellets through the annular area between the experiment vehicle and the wall of the deceleration cart. The average deceleration of the vehicle is 32 g. For the 10-second tests using the accelerator, the cart is deployed after the experiment vehicle clears the top of the cart (see fig. 1). For the 5-second drop tests, the decelerator cart is positioned in the main section of the chamber prior to the test drop. In this study, only the 5-second capability was used.

During the test drop, the experiment falls freely. No guides or lines are connected to the experiment vehicle. The only effective force acting on the freely falling vehicle (viewed from a coordinate system located on the vehicle) is due to residual-air drag. The equivalent gravitational acceleration acting on the experiments during a free-fall test is conservatively estimated to be of the order of magnitude of 10^{-5} g. Data are collected from the experiments by high-speed photography and telemetry. The photographic system

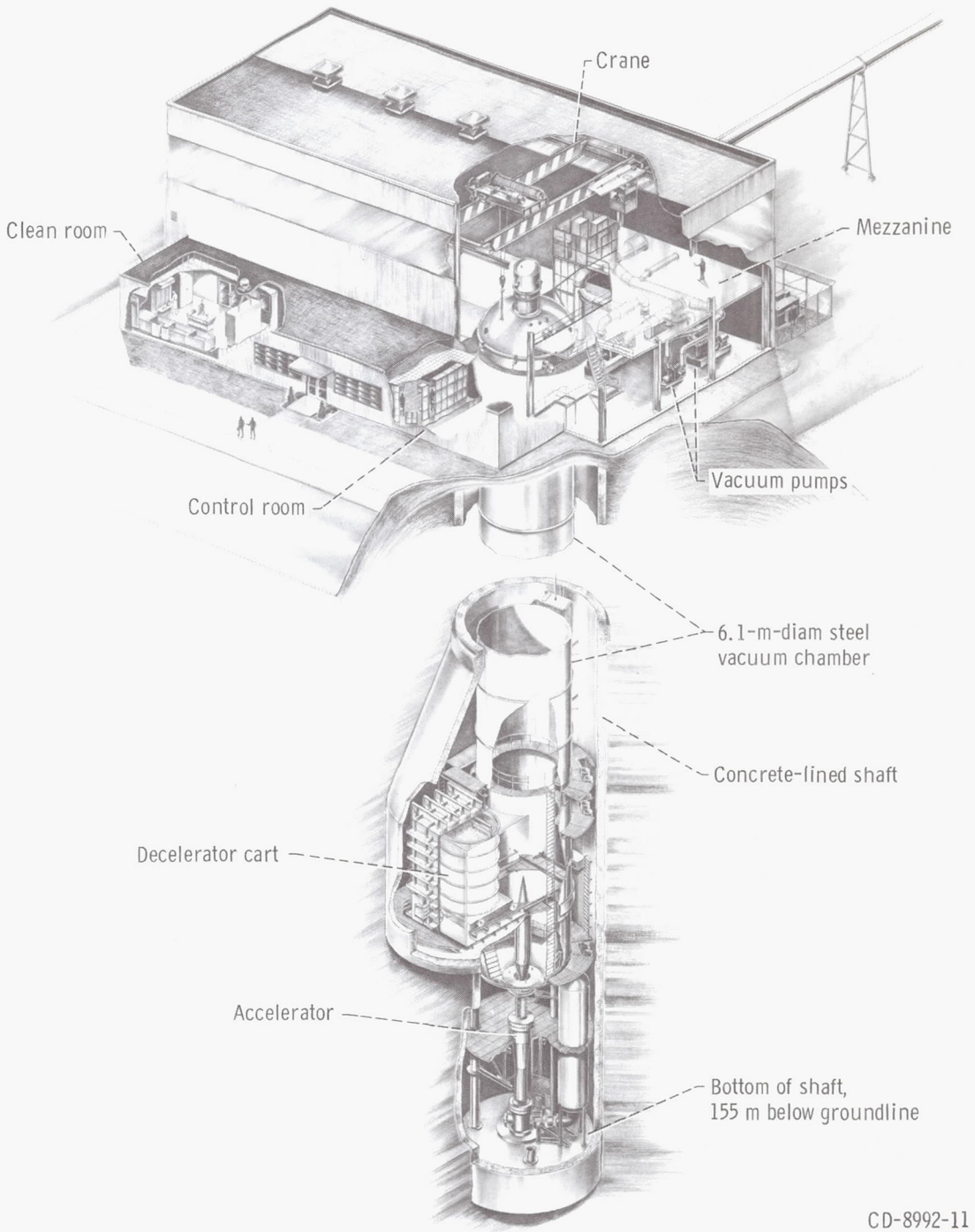

Figure 1. - Schematic view of Zero-Gravity Facility.

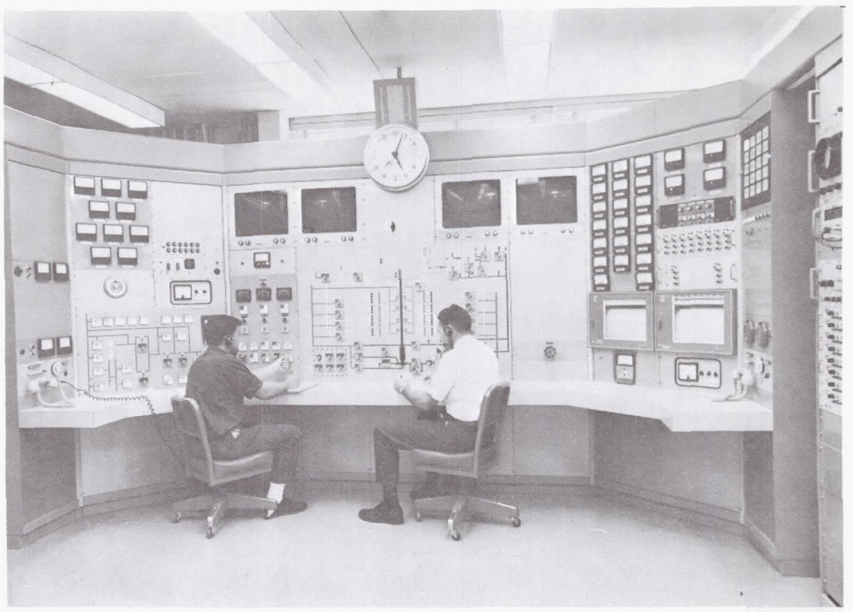

C-67-2568

Figure 2. - Zero-Gravity-Facility control room.

provides as many as 4000 frames per second of high-resolution film data. Telemetry is an Inter-Range Instrumentation Group (IRIG) FM/FM system with 18 continuous channels.

Experiment Vehicle

The experiment vehicle used to obtain the low-gravity data in the Lewis Zero-Gravity Facility is shown in figure 3(a). The height of the vehicle, exclusive of the support shaft, was 2.7 meters, and the largest diameter was approximately 1.06 meters. During this program, the total vehicle mass varied from 750 to 1100 kilograms. The vehicle consisted of three basic sections: a cylindrical body, a conical base containing a thrust system, and a telemetry section.

The vehicle's cylindrical body contained the experiment tray and the electrical power and control system tray. This section was 1.7 meters high, with about 1.1 meters available for the experimental apparatus. The experiment tray is shown in figure 3(b). A direct-current motor supplied a single lateral pulse to a slide carriage which held the test container. A photoelectric displacement transducer supplied measurements of the lateral impulse. Liquid surface motion was recorded photographically at about 400 frames per second. Illumination was by diffuse backlighting. A translucent, graduated scale alongside the test container provided a base for height measurements. Time measurements were obtained by photographing a digital clock and from timing marks

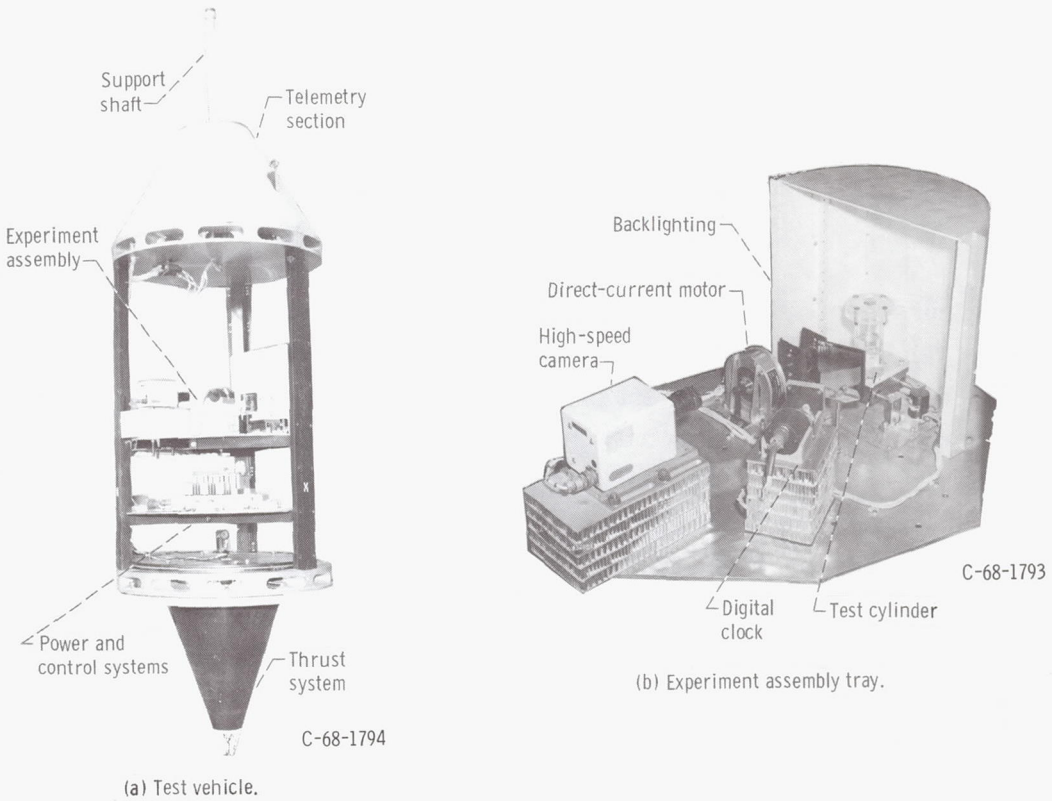

(a) Test vehicle.

(b) Experiment assembly tray.

Figure 3. - Experiment vehicle used for low-gravity tests.

placed on the edge of the data film by a pulse generator. Both time bases were accurate to 0.01 second. During the test drop, the cylindrical section was covered with aluminum side panels to protect the experiment assembly and to aid the vehicle's decelerating characteristics.

The conical base of the experiment vehicle housed a self-contained, cold-gas thrust system. This system produced thrust values ranging from 13 to 130 newtons (3 to 30 lb) for time durations longer than 5 seconds. Steady-state response time was better than 50 milliseconds. The thrust system was calibrated in the facility's main chamber at vacuum levels corresponding to test-drop conditions. The cone was removed from the vehicle and placed on a static thrust calibration stand located in the chamber. A null-balance, load-cell system recorded the thrust-time history. The thrust curves were related to the pressures recorded at the inlet of the thrust nozzle. The magnitude of the thrust was set by changing the nozzle configuration and regulator pressure. The low-gravity acceleration value was also set by adjusting the weight of the vehicle. In this study, low-gravity accelerations produced by the thrust system ranged from about 1 to 18 centimeters per second squared.

The top section of the experiment vehicle contained telemetry. During the test drop,

telemetry was used to continuously record thrust nozzle inlet pressure, two low-gravity accelerometer outputs, and the output of the transducer recording the lateral displacement of the test cylinder. Other telemetric channels were used to monitor general vehicle performance, such as decelerating characteristics.

Test Containers and Liquids

The containers were fabricated from acrylic plastic and precision-diameter, borosilicate glass. The plastic tanks were machined and polished cylinders with hemispherical bottoms. Periodic heat treatment prevented crazing. The glass tanks were cylinders with flat bottoms. They were used only in acquiring deep liquid depth data.

The test liquids and their physical properties pertinent to this study are given in table I. With the exception of the fluorocarbon solvents, these properties were obtained from standard references. The fluorocarbon liquid properties were obtained from unpublished NASA data. The liquids were either analytic reagent grade or, in the case of the fluorocarbon solvents, precision cleaning grade. The liquid temperature was meas-

TABLE I. - SUMMARY OF LIQUID PROPERTIES

AT 20° C

Liquid	Surface tension, σ, dynes/cm[a]	Density, ρ, g/cm^3	Viscosity, η, cP
Acetone	23.7	0.79	0.32
1-Butanol	24.6	.81	2.90
Carbon tetrachloride	26.9	1.59	.97
Ethanol	22.3	.79	1.20
[b]FC-78	13.2	1.72	.82
Methanol	22.6	.79	.60
[c]Freon-TF	18.6	1.58	.70

[a]Where 1 dyne/cm = 1×10^{-5} N/cm.

[b]FC-78 is Minnesota Mining and Manufacturing Co.'s registered trademark for a fluorocarbon solvent.

[c]Freon-TF is E. I. Dupont de Nemours and Co.'s registered trademark for a fluorocarbon solvent (trichlorotrifluoroethane).

ured before each lateral slosh test. Temperature changes were generally small, producing a negligible effect on liquid properties. All liquids had static contact angles of very near 0^{o} on the test cylinder surfaces. A small quantity of dye was added to each liquid to improve photographic quality. The dye had no measurable effect on the pertinent properties of the liquids.

Low-Gravity Test Procedure

The experiment cylinders were prepared in the facility's clean room (fig. 4). Contamination of the liquid and the cylinder surfaces, which could alter the surface tension and contact angle, was carefully avoided. The test cylinders were cleaned ultrasonically in a detergent-water solution, rinsed with a distilled water - methanol solution, and dried in a warm-air dryer. Glassware was precleaned with chromic acid. The cylinders were rinsed with the test liquid, filled to the desired liquid depth, and hermetically sealed in the clean room. Sealing of the test containers not only prevented contamination but was necessary because of the vacuum in the test chamber. The test cylinders were then mounted on the slide carriage in the experiment vehicle.

Electrical timers on the experiment vehicle were set to control the initiation and duration of the lateral impulse. After the remaining vehicle instrumentation (such as the camera, telemetry, etc.) was set, the experiment vehicle was balanced about its vertical

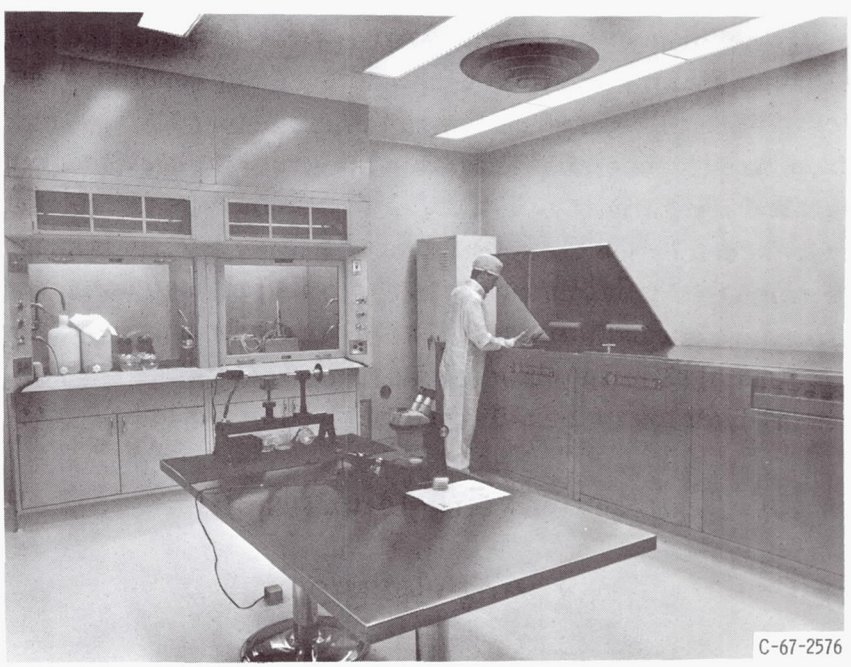

Figure 4. - Zero-Gravity-Facility clean room.

axis. This ensured both an accurate drop trajectory and accurate thrust alinement with respect to the test cylinder. Accurate thrust alinement was necessary to provide an axisymmetric, equilibrium interface shape.

For the drop test, the vehicle was positioned at the top of the vacuum chamber. It was suspended by the support shaft on a hinged-plate assembly. An umbilical cable connected to the top of the support shaft allowed internal measurements, such as liquid temperature and thrust accumulator pressure, to be made during chamber pumpdown. Electrical power was switched to internal a few minutes before vehicle release. The umbilical cable was pneumatically pulled from the support shaft 0.5 second prior to release. The thruster (if used) was activated 0.2 second before release to allow the thrust to reach steady-state conditions. The vehicle was then released by pneumatically shearing a bolt that was holding the hinged plate closed. No measurable disturbances were imparted to the vehicle by this release procedure.

During the test drop, the application of the lateral impulse was preceded by a time delay to allow the liquid-vapor interface to approach its equilibrium shape. This time delay, or formation time t_F, is given in table II for each low-gravity test. The allowed formation time was generally not sufficient to ensure a completely quiescent interface. However, the motion was sufficiently damped that it had no effect on the slosh dynamics. The defined formation time is the total time required to damp out large-amplitude, symmetric slosh oscillations under low-gravity conditions. The initial amplitude of the slosh is the displacement between the normal-gravity liquid surface shape and the low-gravity surface shape. Higher modes are generally excited during the formation.

In this program, total free-fall test time was 5.16 seconds. About 0.13 second before vehicle impact, the thruster was shut down to avoid dispersing the deceleration material. This resulted in about 5 seconds of usable low-gravity test time with thrust. The vehicle's trajectory and deceleration were monitored by closed-circuit television. Following the test drop, the chamber was opened to atmospheric pressure and the vehicle was returned to ground level (fig. 5).

The low-gravity acceleration values were obtained from the ground calibration curves of the experiment vehicle's thrust system to within ±6 percent. Telemetry data during the test drop were used to corroborate the calibrated thrust values. Both the nozzle pressure and the low-gravity accelerometer output were telemetered and recorded during the test drop. These data were then compared with the preset ground calibration data. Ground calibration was used for the low-gravity acceleration values because it was more accurate than the accelerometer telemetry data.

TABLE II. - SUMMARY OF LOW-GRAVITY DATA

Liquid	Cylinder radius, R, cm	System acceleration, a, cm/sec^2	Bond number, Bo	Normalized liquid depth, h/R	Formation time, t_f, sec	Measured natural frequency, ω_1, rad/sec	Logarithmic decrement, δ
Acetone	1.59	0.0098	0.0008	>2.0	0.88	4.68	0.55
	1.59	1.08	.09	↓	.80	4.32	.51
	1.90	.0098	.0012		.88	3.53	.58
	2.22	.0098	.0016		1.10	2.66	----
	2.54	.0098	.0021		1.45	1.96	----
1-Butanol	1.90	0.0098	0.0021	>2.0	0.86	3.83	1.20
Carbon tetrachloride	1.59	0.0098	0.0015	>2.0	0.88	3.43	0.85
	1.59	5.87	.88	>2.0	1.00	4.29	.67
	2.00	9.30	2.21	1.0	1.25	3.74	----
[a]FC-78	1.90	17.6	8.4	>2.0	1.42	4.05	0.52
	2.22	17.6	11.4	>2.0	1.44	4.01	.45
	2.50	17.6	14.5	.25	1.50	2.83	----
	2.54	17.6	14.9	>2.0	1.32	3.70	----
Methanol	2.00	11.8	1.6	0.25	1.00	2.68	----
	2.00	11.8	1.6	.50	1.00	3.80	----
[b]Freon-TF	2.00	11.8	4.0	0.25	1.25	2.33	----
	2.00	11.8	4.0	.75	1.50	3.39	----
	2.50	17.6	9.3	.25	↓	2.47	----
	2.50	17.6	9.3	.50		3.19	----
	2.00	17.6	6.0	>2.0		4.35	0.46

[a]FC-78 is Minnesota Mining and Manufacturing Co.'s registered trademark for a fluorcarbon solvent.

[b]Freon-TF is E. I. Dupont de Nemours and Co.'s registered trademark for a fluorocarbon solvent (trichlorotrifluoroethane).

Figure 5. - Vehicle retrieved following test drop.

Normal-Gravity Lateral Slosh

The apparatus used to obtain the normal-gravity data for this study is shown in figure 6. This slosh apparatus can supply a variety of forcing functions over a range of frequencies and amplitudes applicable to lateral sloshing. The lateral drive is supplied by a high-torque, variable-speed, direct-current motor. The cam shape determines the form of the forcing function. In this study, the forcing function was essentially a single pulse. The amplitude and duration of the pulse were experimentally set to produce small-amplitude, normal-mode lateral sloshing. The experiment tanks were cleaned and prepared in the same way as for the low-gravity tests. A high-speed camera recorded the fluid behavior. A digital clock with a calibrated accuracy of 0.01 second was placed in the field of view of the camera to provide time measurements.

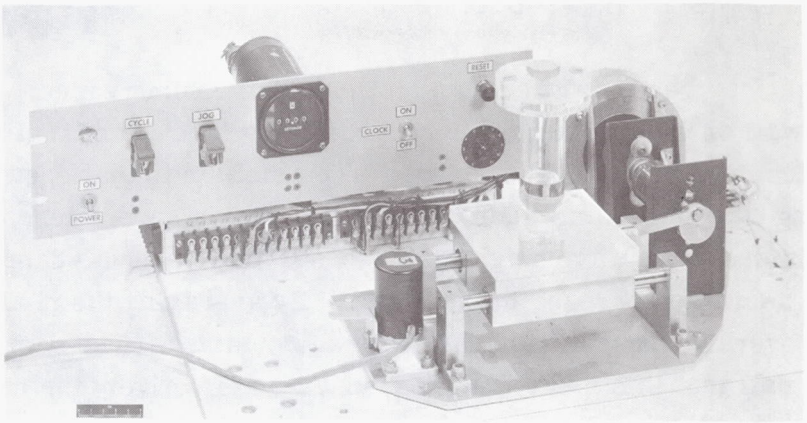

C-67-4074

Figure 6. - Lateral slosh apparatus for normal-gravity tests.

RESULTS AND DISCUSSION

The dimensionless parameter that characterizes a low-gravity condition for a fluid interface system is the Bond number. The Bond number for a cylindrical tank is

$$Bo = \frac{aR^2}{\beta} \tag{1}$$

where a is the equivalent gravitational acceleration. When the Bond number is large, gravity dominates; when small, capillarity dominates. Thus, the acceleration, system size, and fluid properties are all necessary to characterize a low-gravity fluid condition.

In this study, the maximum Bond number during a free-fall drop was 0.002. This value is based on the estimated acceleration value of 10^{-5} g. The majority of free-fall drops resulted in Bond numbers of approximately 0.001. Bond numbers of this order of magnitude are referred to as zero. Similarly, the terms "high" Bond number and "low" Bond number will refer to Bond numbers greater than and less than 100, respectively. These definitions are arbitrary and are not to be regarded as exact quantitative boundaries, especially at shallow liquid depths. The definitions of high, low, and zero Bond numbers are used herein only for convenience in describing general limitations of theoretical analyses and sets of experimental data.

The low-gravity data obtained in the Lewis Zero-Gravity Facility resulted in Bond numbers ranging from 0 to about 15 with cylinder radii ranging from 1.59 to 2.54 centimeters. The data obtained at normal gravity using cylinder radii between 0.317 and 3.17 centimeters resulted in Bond numbers ranging from about 3 to 800.

Data Reduction

The film slosh data were analyzed on a motion picture film reader. Slosh wave heights along the wall of the cylinder were recorded as a function of time. These data were plotted by a computer printout, yielding curves similar to that shown in figure 7. All lateral sloshing was small amplitude, that is wave heights were less than 0.25 R. For these small amplitudes, wall wave heights were observed to execute damped harmonic motion with no measurable decrease in frequency. By averaging the plotted half-periods of oscillation, an overall frequency for each test was obtained. The damping in all cases was sufficiently small that this measured frequency was effectively the natural frequency ω_1. The damping was observed to be exponential and thus can be described in terms of the logarithmic decrement δ. The logarithmic decrement was obtained by plotting the amplitude decay per cycle (ref. 4).

The value of the centerline liquid depth h depends on the magnitude of the Bond number, as well as on the liquid volume. For the zero and high Bond number extremes, the centerline liquid depth is related simply to the volume of the liquid. At other Bond numbers, relations similar to that given on page 96 of reference 6 may be used to relate the centerline depth to liquid volume. The latter theoretical curves were used to initially determine the liquid volume required to yield a desired liquid depth at a given Bond number. The liquid depth was also measured directly from the data film. No measurable discrepancies were noted.

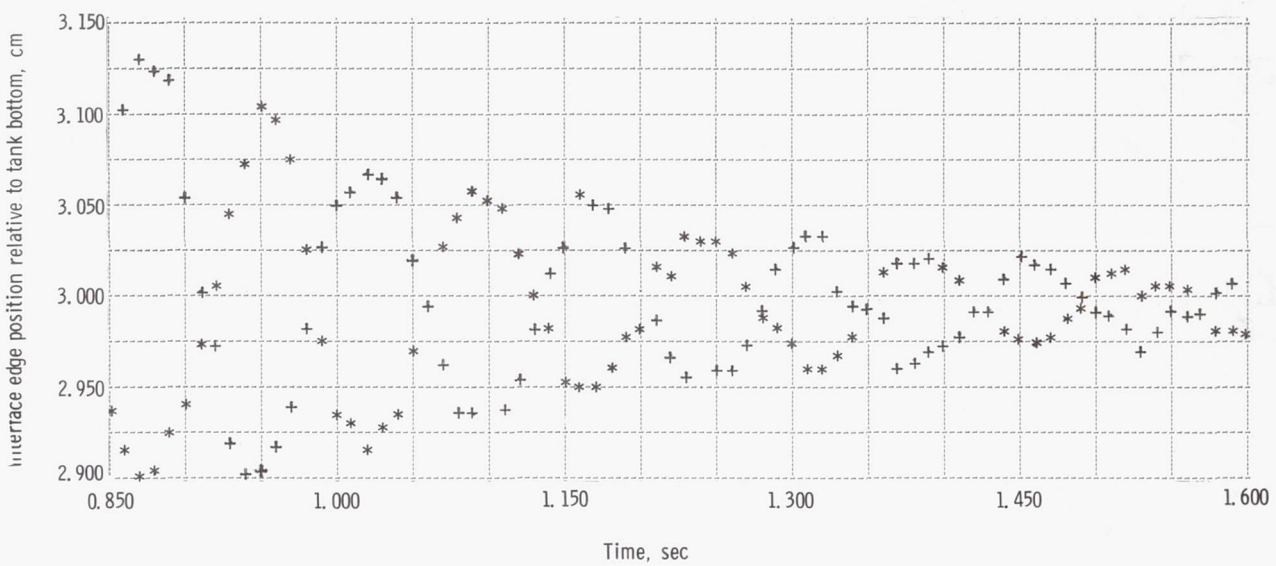

Figure 7. - Sample data plot of lateral slosh. Bond number, 29.

Fundamental Mode Shape

Representative photographs of the first or fundamental lateral slosh mode at various Bond numbers are shown in figure 8. The normal- and low-gravity data extend over a range of Bond numbers from 0 to about 800. The equilibrium liquid surface correspondingly ranged from a hemispherical to an essentially flat surface shape. As might be expected, the fundamental slosh-mode shape exhibits a similar dependence on Bond number. In the fundamental mode, the vertex of the liquid surface remains at the centerline of the cylinder and maximum displacement occurs at the cylinder wall (see fig. 9). Quantitative measurements of the mode shape could not be obtained accurately in this study, principally because of refraction effects near the wall of the cylinder. However, the mode shapes (0° static contact angle) did agree qualitatively with the theoretical eigenmodes (5° static contact angle) given in reference 6. Higher modes were generally excited during the application of the lateral impulse. Only rarely was circular motion or swirling observed. In all cases these higher and nonlinear modes quickly decayed to the fundamental mode during the free lateral sloshing.

Free lateral sloshing was observed to occur on a thin layer of liquid rather than on an unwetted surface. The initial slosh wave deposits a film of liquid on the wall. Subsequent oscillations occur on this liquid film. This observation was previously noted by the authors for lateral sloshing at zero Bond numbers (ref. 4). While this residual layer is especially noticeable at low Bond numbers (apparently being more pronounced for liquids with the lowest surface tensions), the residual liquid layer was observed over the entire Bond number range of this study.

This fact is important for several reasons. It may explain the agreement between inviscid theory and experimental results obtained in cylinders of relatively small diameter. The residual layer may influence the sloshing characteristics, either directly or indirectly through possible changes in the contact angle. Contact-angle changes, whether hysteresis, dynamic, or the reported "stuck"-edge effect (ref. 1), are known to influence the natural frequency. Recently, Miles has proposed that contact-angle effects may partly explain the small but measurable differences between theoretical and experimental damping at large Bond numbers (ref. 7). It might be expected that these effects would be greater in low-Bond-number environments because of the relatively greater role of capillarity. The residual liquid layer is important in determining the magnitude of these effects.

A discussion of the possible contact-angle effects (considering the residual liquid film) is given later (p. 30). It is sufficient to say that fundamental lateral sloshing obtained in this study was "free," that is, there were no measurable contact-angle variations. The apparent curvature of the sloshing-mode shape increased smoothly from the vertex to the edge. This was an experimental condition for this program. Experiment

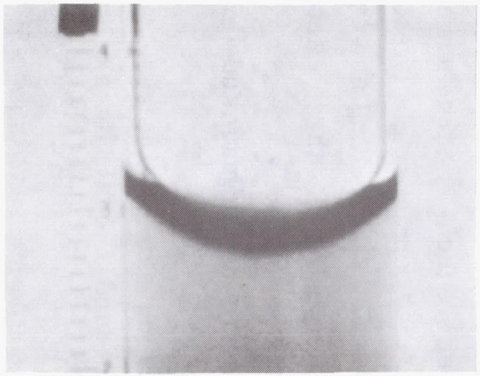

(a) Bond number, <0.001; acceleration, 0.0098 centimeter per second squared; cylinder radius, 1.90 centimeters.

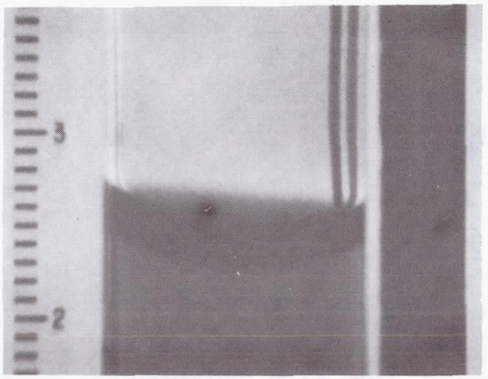

(b) Bond number, 0.9; acceleration, 1.59 centimeters per second squared; cylinder radius, 1.59 centimeters.

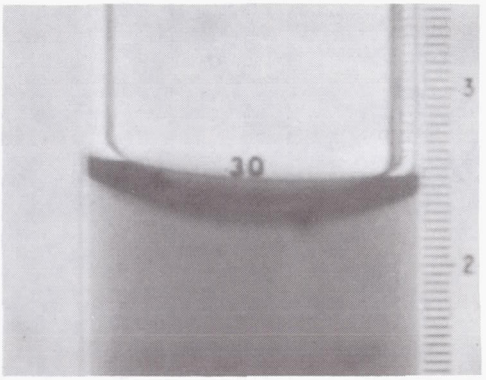

(c) Bond number, 6; acceleration, 17.6 centimeters per second squared; cylinder radius, 2.0 centimeters.

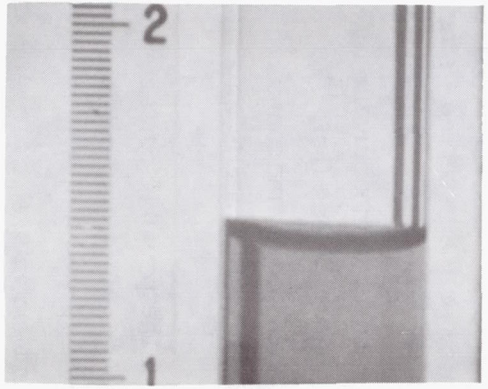

(d) Bond number, 13; acceleration, 980 centimeters per second squared; cylinder radius, 0.635 centimeter.

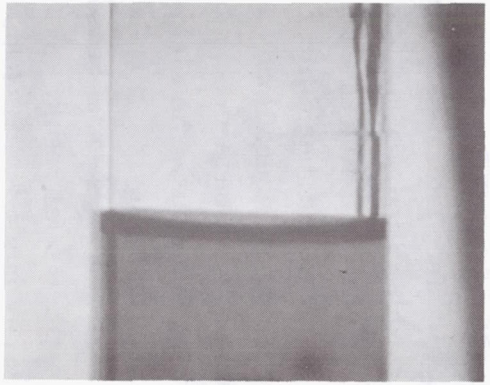

(e) Bond number, 30; acceleration, 980 centimeters per second squared; cylinder radius, 0.952 centimeter.

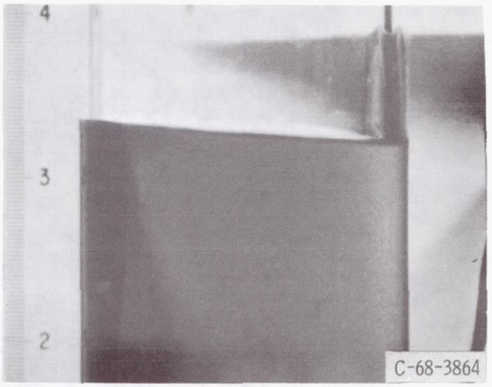

(f) Bond number, 536; acceleration, 980 centimeters per second squared; cylinder radius, 2.54 centimeters.

Figure 8. - Fundamental sloshing mode at various Bond numbers.

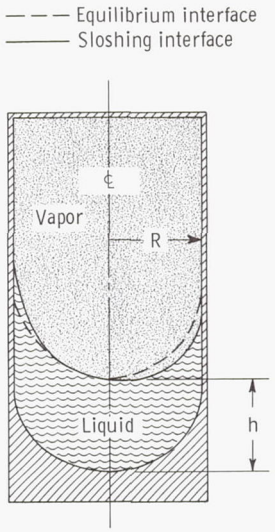

Figure 9. - Test geometry.

parameters were selected deliberately to allow free oscillations and to avoid introducing contact-angle changes.

Natural Frequency

Deep liquid depth ($h/R > 2$). - The natural frequency data obtained in this study at deep liquid depths are given in tables II and III. The natural frequency ω_1 can be expressed in the dimensionless form

$$\Omega^2 = \frac{\omega_1^2 R^3}{\beta} \tag{2}$$

A plot of the data in the form of equation (2) as a function of Bond number is presented in figure 10. Note that the Bond number coordinate is Bo + 1.4. This choice of scale permits the zero Bond number data to be placed on the log-log graph and also facilitates a graphical solution to the data (see p. 20). The low- and normal-gravity data are separately indicated. These show that there are no separate trends and that the scaling parameters were correctly chosen. Also, at comparable Bond numbers the low-gravity data have generally larger cylinder radii than the normal-gravity data.

The zero Bond number point in figure 10 is the average of the data obtained in this study and the data previously presented in reference 4. The results of this investigation using larger radii cylinders and longer environment test times than previously available

TABLE III. - SUMMARY OF NORMAL-GRAVITY DATA

Liquid	Cylinder radius, R, cm	Normalized liquid depth, h/R	Measured natural frequency, ω_1, rad/sec	Logarithmic decrement, δ	Bond number, Bo
Acetone	0.317	>2.0	92.4	0.66	3.4
	.635	↓	55.6	.18	13
	.952		44.2	.16	30
	1.59		32.7	.06	82
	1.90		30.5	.05	118
1-Butanol	0.317	>2.0	88.4	1.39	3.2
	.635	↓	55.8	.64	13
	.952		43.3	.33	29
	1.27		37.4	.40	52
Carbon tetrachloride	0.317	>2.0	84.9	0.64	5.9
	.500	.25	43.3	----	15
	.500	.50	36.9	----	15
	.635	>2.0	54.1	.27	24
	.952	>2.0	44.2	.16	53
	1.00	.25	32.4	----	58
	↓	.50	32.9	----	58
		.75	35.5	----	58
		1.00	38.3	----	58
	1.27	>2.0	37.6	.10	94
Ethanol	0.317	>2.0	89.7	0.96	3.5
	.635	↓	53.9	.34	14
	.952		43.6	.41	31
	1.58		33.0	.14	86
	2.22		28.3	.11	171
	3.17		22.4	.07	348
Methanol	0.317	>2.0	92.9	0.75	3.5
	.500	.25	39.2	----	8.6
	↓	.50	51.5	----	↓
		.75	56.1	----	
		1.00	61.0		
	.635	>2.0	55.6	0.25	14
	.750	.25	33.9	----	19
	.750	.75	42.7	----	19
	.952	>2.0	43.6	0.25	31
	1.00	.25	31.0	----	34
	1.00	.50	34.3	----	34
	1.25	.25	28.2	----	54
	1.25	.50	29.8	----	54
[a]Freon-TF	0.317	>2.0	78.5	----	8.3
	.500	.50	46.2	----	21
	.500	1.00	56.1	----	21
	.635	>2.0	53.7	0.18	33
	.952	>2.0	43.0	.13	75
	1.25	.25	28.6	----	130
	↓	.50	29.9	----	↓
		.75	32.0	----	
		1.00	34.5	----	
	1.27	>2.0	37.4	0.07	134
	1.58	>2.0	33.0	.06	207
	1.90	>2.0	30.8	.06	300
	2.00	.25	22.4	----	330
	↓	.50	23.9	----	↓
		.75	25.4	----	
		1.00	27.3	----	
	2.54	>2.0	26.3	0.03	536
	3.17	>2.0	24.0	.03	835

[a]Freon-TF is E. I. Dupont de Nemours and Co.'s registered trademark for a fluorcarbon solvent (trichlorotrifluoroethane).

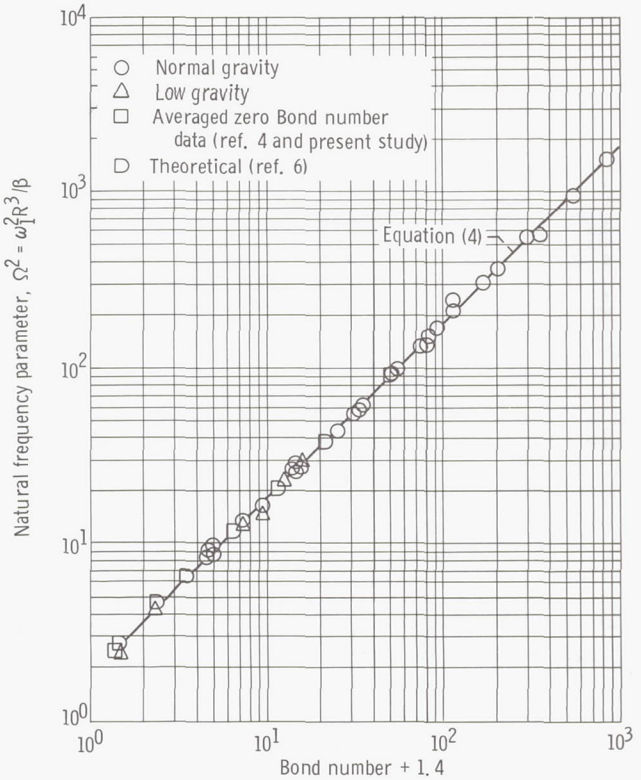

Figure 10. - Correlation of natural frequency with Bond number. Liquid depth ratio, >2.

confirm that $\Omega^2 = 2.6$ ($\theta_s = 0^o$) at zero Bond numbers.

The theoretical points shown in the figure were calculated from the eigenvalues ($\theta_s = 5^o$) presented in reference 6. While the theoretical points are consistently above the experimental data below Bond numbers of 10, the theoretical calculations agree quite well with the data. Specifically, the largest difference is at a Bond number of 0 where the theoretical Ω^2 is 2.8. This difference is less than 8 percent. The data adequately confirm the theoretical calculations at deep liquid depths, considering experimental error and the differences in contact angle.

When the zero Bond number result ($\Omega^2 = 2.6$) and the known natural frequency relation for large Bond numbers at deep liquid depth, namely,

$$\left.\begin{aligned} \omega_1^2 &= 1.84\,\frac{a}{R} \\ \text{or} \\ \Omega^2 &= 1.84\ \text{Bo} \end{aligned}\right\} \qquad (3)$$

are used, the relation that best describes all the data in figure 10 is

$$\left.\begin{aligned} \Omega^2 &= 1.84(1.4 + \mathrm{Bo}) \\ \Omega^2 &= 2.6 + 1.84\ \mathrm{Bo} \end{aligned}\right\} \qquad (4)$$

or

$$\omega_1^2 = (2.6 + 1.84\ \mathrm{Bo})\frac{\sigma}{\rho R^3} \qquad \frac{h}{R} \geq 2,\ \theta_s = 0^o$$

Equation (4) is represented by the straight line in figure 10. The difference between this result and others previously presented is the constant 2.6. Others have used 1.5, the number originally estimated by Satterlee and Reynolds (ref. 1, chapter 11). The constant 2.6 represents the capillary contribution to the lateral natural frequency. Equation (4) shows that capillary effects begin to appear for Bond numbers below about 20. Since the correlation reduces to the confirmed high Bond number results, equation (4) is valid at all Bond numbers.

Shallow liquid depth ($h/R < 2$). - At all Bond numbers, the natural frequency decreases as the liquid depth decreases. The shape of the cylinder bottom determines the depth dependence of the natural frequency. For flat-bottom cylinders, results given in references 1, 3, and 5 cover the entire Bond number range. For hemispherical-bottom cylinders, only the Bond number extremes have been studied experimentally. At zero Bond numbers, the relation obtained was (ref. 5)

$$\omega_1^2 = \frac{2.6\,\beta}{R^3}\tanh\left(2\frac{h}{R}\right) \qquad \theta_s = 0^o \qquad (5)$$

At high Bond numbers, spherical-tank eigenvalues at discrete liquid depths were calculated by Budiansky (ref. 8) and independently by Riley (ref. 9). Their results with $h/R \leq 1$ can be used to calculate frequencies in hemispherical-bottom tanks at high Bond numbers. Their results are in agreement with published normal-gravity experimental data.

The shallow liquid depth, natural frequency data in hemispherical-bottom cylinders obtained in this study are given in tables II and III. These data cover the Bond number range from 1.6 to 330. Only data above liquid depth ratios of 0.25 were obtained. Accurate measurements of natural frequency could not be made below this depth ratio. By using the natural frequency parameter defined by equation (2), the data were plotted in figure 11(a) to (d) at the four liquid-depth ratios studied. The half-power of the frequency parameter was used to avoid squaring errors in the measured frequency. The zero Bond

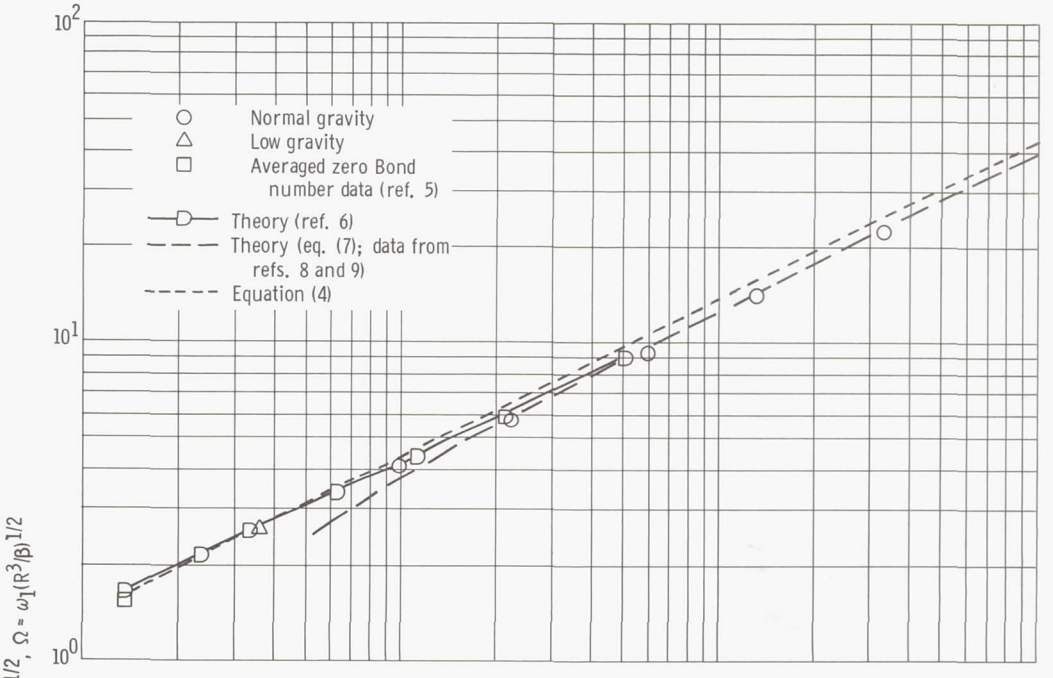

(a) Liquid depth ratio, 1.00.

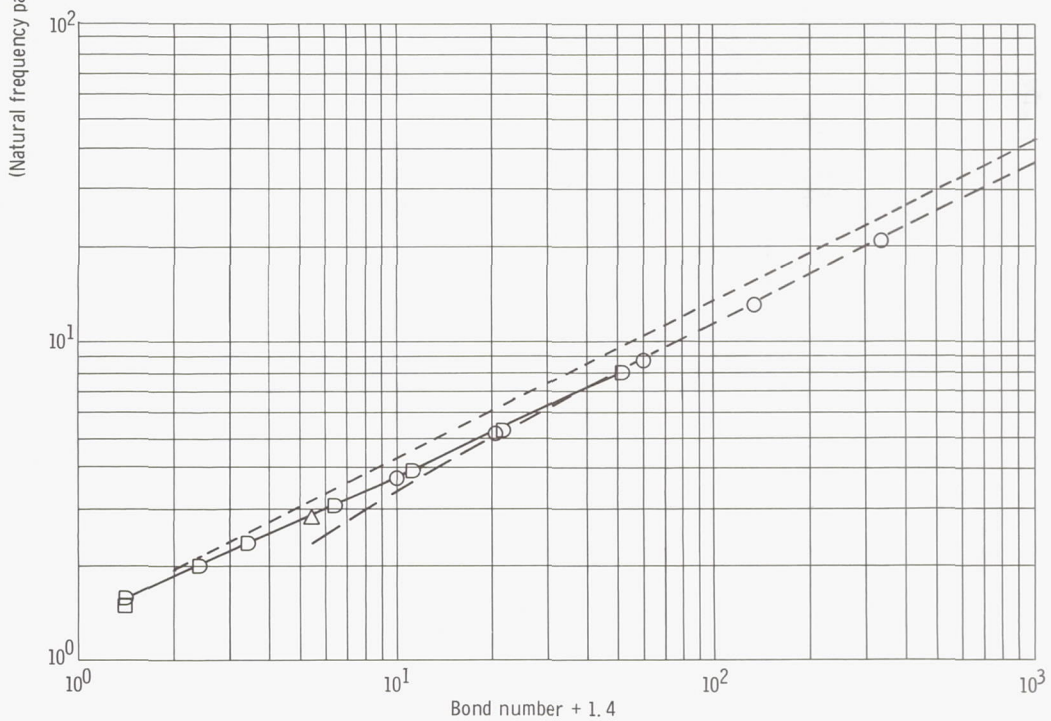

(b) Liquid depth ratio, 0.75.

(Natural frequency parameter)$^{1/2}$, $\Omega = \omega_1 (R^3/\beta)^{1/2}$

Figure 11. - Natural frequency parameter as function of Bond number.

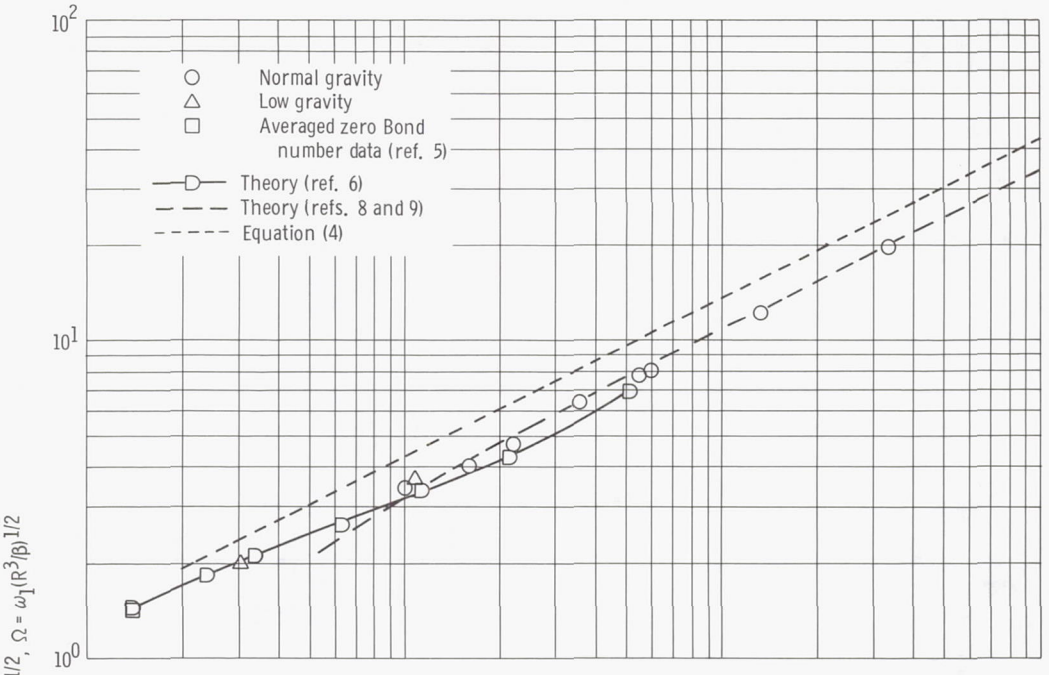

(c) Liquid depth ratio, 0.50.

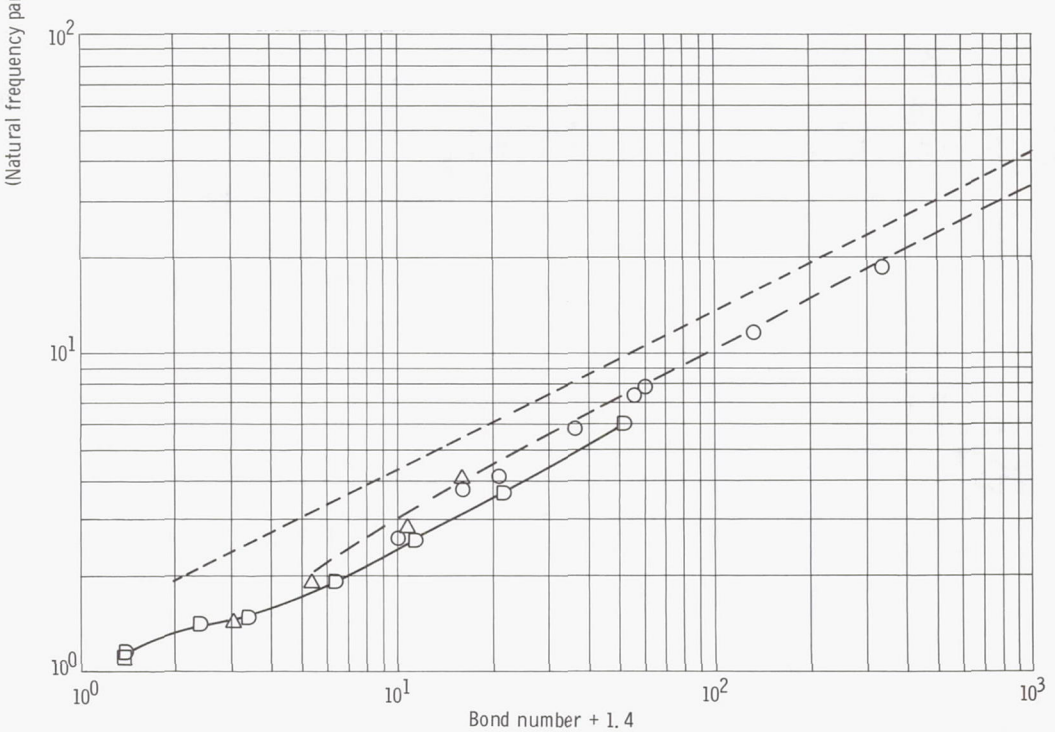

(d) Liquid depth ratio, 0.25.

Figure 11. - Concluded.

number points were obtained from reference 5.

The theoretical low Bond number points calculated from the eigenvalues given in reference 6 are also shown in these plots. Points at the liquid depth ratio of 0.75 were extrapolated from these calculations. These points have been connected by a hand-drawn, solid curve. The large-dashed curves represent theoretical values interpolated from the results of Budiansky and Riley (refs. 8 and 9). The fundamental eigenvalue λ_1 of their studies is

$$\lambda_1 = \frac{\omega_1^2 R}{a} \tag{6}$$

This equation can be written in the form

$$\Omega = (\lambda_1 Bo)^{1/2} \tag{7}$$

allowing direct comparison with the experimental data and low Bond number theory. The large-dashed curves in figure 11 are plots of equation (7) with the appropriate values for λ_1. The specific values were $\lambda_1 = 1.56$ for $h/R = 1.00$, 1.35 for $h/R = 0.75$, 1.19 for $h/R = 0.5$, and 1.075 for $h/R = 0.25$. These curves are extended down to Bond numbers of 4. This extension is not intended to provide low Bond number predictions, as equation (7) is rigorously valid only for flat equilibrium liquid surfaces, where capillarity can be ignored. However, the experimental data and low Bond number theory should approach these curves as the Bond number increases. The high Bond number curves were therefore arbitrarily extended to show asymptotic trends.

The data agree with theory in that the frequency does not decrease significantly until the liquid depth ratio is below 1.0. The decrease in frequency caused by reducing the liquid depth ratio from 2.0 to 1.0 is less than 10 percent (see small-dashed curve in fig. 11). Below a depth ratio of 1.0, the frequency decrease occurs rapidly.

In figure 11, the experimental data at shallow liquid depths are shown to agree with the analytical results of Concus (ref. 6) at low Bond numbers and Budiansky and Riley (refs. 8 and 9) at high Bond numbers. At liquid depth ratios of 1.0 and 0.75, the theoretical curves become asymptotic at Bond numbers of 40 to 50. There is a trend towards a higher asymptotic Bond number value at the lower liquid depth ratios. Near these values the experimental data begin to fall towards the low Bond number theoretical curves. These asymptotic Bond number values agree qualitatively with the change in the shape of the equilibrium liquid surface with Bond number. For deep liquid depths, the liquid surface is reasonably flat at Bond numbers as low as about 50. For shallow liquid depths, where both Bond number and liquid volume are necessary to characterize the liquid sur-

face shape, a larger Bond number is required to produce a flat liquid surface.

The low Bond number theoretical curve is not smooth at the liquid depth ratio of 0.5. At the 0.25 depth ratio, inflections in the theoretical curve are even greater. A comparison between the theoretical eigenvalues and the data at this depth ratio (0.25) is made in figure 12. The low Bond number eigenvalues $\omega_1^2/[(1 + Bo)\beta/R^3]$ were obtained directly from the results of reference 6. These eigenvalues reduce to the normal-gravity eigenvalue form given in equation (6) at large Bond numbers. The square roots of the eigenvalues are plotted in figure 12, again to avoid multiplying error in the measured frequency.

The data and theoretical eigenvalues for the liquid depth ratio of 1.0 are also presented in figure 12 for comparison. At this depth ratio, the low and high Bond number eigenvalues and the experimental data are in agreement. The eigenvalues display a smooth decrease from the zero Bond number value, asymptotically approaching the high Bond number eigenvalue at a Bond number of 50. The 0.75 depth ratio data show a similar trend. The 0.50 depth ratio data are similar to that shown by the presented 0.25 depth ratio data. Here, the calculated zero Bond number eigenvalue is also greater than the high Bond number eigenvalue. However, as the Bond number increases the eigenvalues drop below the high Bond number value.

The experimental data tend toward the high Bond number eigenvalue faster than the calculated low Bond number eigenvalues at the liquid depth of 0.25. At a Bond number of 50, the difference between the data and low Bond number theory is about 20 percent. This is the largest difference noted (regardless of liquid depth ratio). The experimental data do, however, follow the inflection in the analytical low Bond number curve. It can be concluded that the experimental data agree with the low Bond number theory over the range of liquid depths studied, considering the measurement error and difference in contact angle.

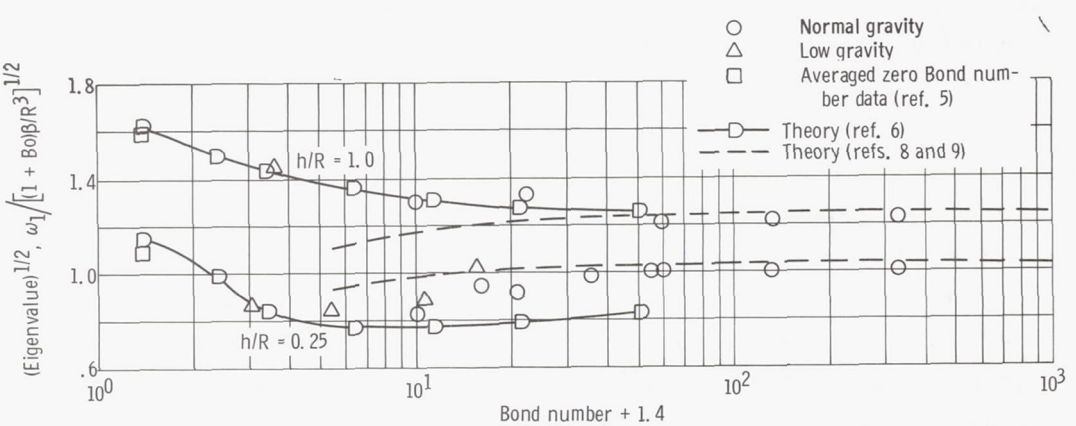

Figure 12. - Comparison of experimental data with theoretical eigenvalues.

Deep Liquid Depth Damping

Logarithmic decrement results. - The decay of the lateral slosh wave at the wall of the cylinder was measured in terms of the logarithmic decrement. The logarithmic decrement is defined as

$$\delta = \frac{1}{n} \ln \frac{A_0}{A_n} \tag{8}$$

and is related to the exponential damping coefficient α by

$$\delta = \frac{2\pi\alpha}{\omega_1} \qquad \omega_1 \approx \omega_d \tag{9}$$

The experimental logarithmic decrement data obtained in this study are given in tables II and III. These data represent the total damping observed for each set of variables. Values are given only for the deep liquid depth data. At shallow liquid depths, measurements of δ based on equation (8) were found to contain too large an uncertainty to be reliable.

The logarithmic decrement may be expressed in terms of the system variables by

$$\delta = K_d \left(\frac{\eta}{\rho \omega_1 R^2} \right)^{1/2} \tag{10}$$

The empirical value of K_d is 6.1 for high Bond numbers (refs. 1 and 10) and 28.1 for zero Bond numbers (ref. 4). A plot of the experimental data, expressed as K_d, is shown in figure 13 as a function of Bond number. The K_d values were calculated by using equation (10) and the measured frequencies and logarithmic decrements. Note that the abscissa is the square root of the Bond number. Representative zero Bond number data (i.e., $Bo < 0.001$) from reference 4 are included in figure 13. The zero Bond number data are shown separately to indicate the spread in the measured values. The zero Bond number value of $K_d = 28.1$ obtained in reference 4 is an average result accurate to within ±10 percent. The data obtained in this study are within this average value. Therefore, these results, using larger-radii cylinders and a longer environmental test time than previously, confirm that $K_d = 28.1$ at zero Bond numbers.

In figure 13, it is shown that equation (10), with K_d regarded as an explicit function of Bond number, represents a satisfactory correlation of the data. There are no separate trends with either acceleration or fluid property dependence. The data are ap-

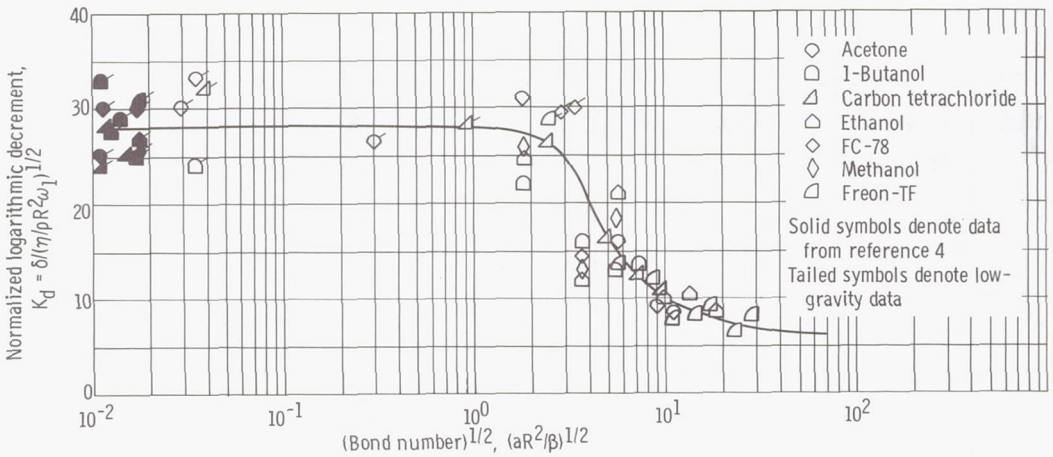

Figure 13. - Low-gravity and normal-gravity experimental damping data.

proaching the required value of $K_d = 6.1$ at high Bond numbers. By using this value and the zero Bond number result, a curve was fitted to the data. This curve is shown in figure 13. The curve represents a reasonable approximation to the data and can be used to predict the total damping of free, fundamental lateral sloshing at any Bond number.

The increase in the coefficient of the logarithmic decrement (i. e., K_d) over the high Bond number result occurs in the same Bond number region where the interface shape changes rapidly. An attempt was made to correlate the logarithmic decrement curve with the shape of the interface, but no satisfactory relation was obtained. Nevertheless, we believe that the change in shape of the interface has an effect on the observed change in damping and that the damping over the entire Bond number spectrum is due principally to viscous effects at the wall of the cylinder.

Besides viscous damping at the container wall, the total damping may also be caused by bottom effects, contact-angle variations, and surface damping (ref. 7). Damping due to bottom effects was negligible because of the deep liquid depth ratios. The effect of possible contact-angle variations is discussed later (p. 30). Surface damping was observed to affect the higher modes. (These higher modes were more quickly damped at lower Bond numbers.) However, we believe that surface damping is negligible in the fundamental mode. Surface-tension variations and contamination were precluded by the choice of liquids and cleaning procedures used in this study. Therefore, the total damping in the fundamental mode is principally due to viscous damping at the container wall. An increase in viscous damping occurs as the Bond number decreases and the interface becomes more curved; a constant limit is reached when the interface shape is nearly hemispherical.

Comparison with published results. - The damping data of this study may be compared with the normal-gravity results of Clark and Stephens (ref. 2) and Dodge and Garza

(ref. 3). The relation obtained by Clark and Stephens may be written as

$$\delta = 6.1\left(\frac{\eta}{\rho\omega_1 R^2}\right)^{1/2} + 0.60\ \mathrm{Bo}^{-3/5} \tag{11}$$

The relation proposed by Dodge and Garza is

$$\delta = 6.1\left(\frac{\eta}{\rho\omega_1 R^2}\right)^{1/2}\left(1 + 8.20\ \mathrm{Bo}^{-3/5}\right) \tag{12}$$

Both equations (11) and (12) were empirically obtained, the former by visual measurements (i.e., using eq. (8)) and the latter by force response measurements. While each reduces to the confirmed value of K_d at high Bond numbers, neither relation correctly predicts the logarithmic decrement at very low Bond numbers.

These results are compared directly with the results of this study in figure 14. The solid curve was previously presented in figure 13. The dashed curve represents equation (12); the corresponding data are also from the same study. (Neither eq. (11) nor the actual data presented by Clark and Stephens can be plotted in the form used in the figure. It is noted, however, that eq. (12) was also found to fit their data.) Some high Bond number data obtained by Stephens are also shown. Except for very low Bond numbers, figure 14 shows that the studies yield similar results. The data spread is about the same as that occurring at high Bond numbers. Specifically, the magnitudes of the logarithmic decrement at any given Bond number are comparable. The rates of change in the logarith-

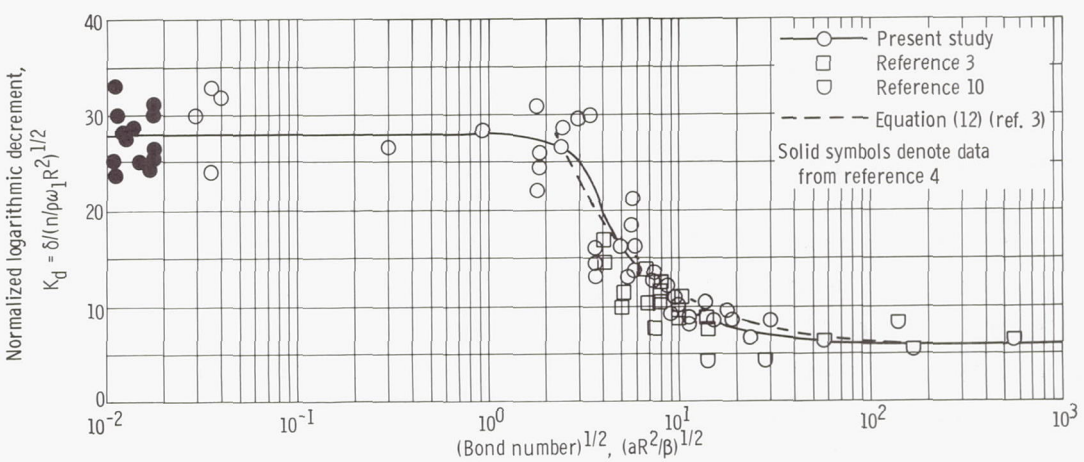

Figure 14. - Comparison of published damping data.

mic decrements are nearly identical and occur in the same Bond number region.

Damping coefficient. - From equation (9) the damping coefficient is

$$\alpha = \frac{\delta \omega_1}{2\pi} \tag{13}$$

The coefficient of the logarithmic decrement increases by a factor of 4 from high to zero Bond numbers. However, the natural frequency decreases. The behavior of the damping coefficient as a function of Bond number depends on these two opposing changes. Substituting the correlations for δ and ω_1 (eqs. (4) and (10)) into equation (13) yields

$$\alpha = \frac{K_d}{2\pi}\left(\frac{\eta}{\rho R^2}\right)^{1/2}\left[(2.6 + 1.84\ \mathrm{Bo})\frac{\sigma}{\rho R^3}\right]^{1/4} \qquad \frac{h}{R} \geq 2,\ \theta_s = 0^o \tag{14}$$

where K_d is an explicit function of Bond number given by the curve in figure 13. This equation can be used to predict the total damping coefficient at deep liquid depth ratios. Normalizing equation (14) by using α at zero Bond numbers, that is,

$$(\alpha)_{Bo=0} = \frac{28.1}{2\pi}\left(\frac{\eta}{\rho R^2}\right)^{1/2}\left(2.6\frac{\sigma}{\rho R^3}\right)^{1/4} \tag{15}$$

eliminates the explicit radius and liquid property dependence

$$\frac{\alpha}{(\alpha)_{Bo=0}} = \frac{K_d(2.6 + 1.84\ \mathrm{Bo})^{1/4}}{35.7} \tag{16}$$

In this form, the normalized damping coefficient is an explicit function of Bond number only.

The normalized damping coefficient given by equation (16) and the experimental data of this study are plotted in figure 15. The data were plotted by using the actual measured frequency and decrement values. The normalized damping coefficient curve has a relative maximum at a Bond number of about 9. This is caused by the empirical curve used to correlate K_d. The natural frequency increases continuously with Bond number; K_d, however, displays a step decrease in the Bond number region of about 1 to 100. For Bond numbers from 1 to 9, ω_1 increases faster than the decrease in K_d. For Bond numbers from 9 to 100, K_d dominates and decreases faster than the increase in ω_1.

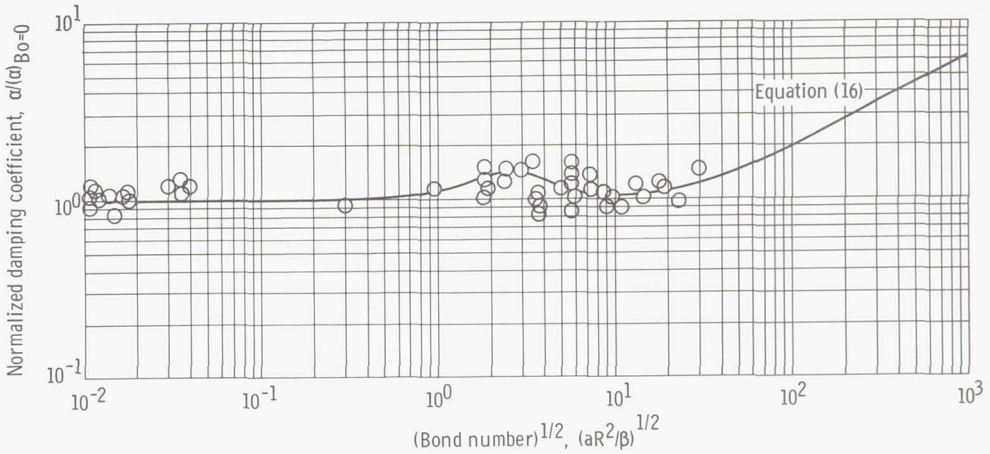

Figure 15. - Damping coefficient as function of Bond number.

Above Bond numbers of about 100, where K_d approaches a constant, the normalized damping coefficient increases continuously with ω_1.

Since the curve for K_d in figure 13 is only an approximation, the exact nature of the inflection in the normalized damping coefficient is uncertain. However, the average of the data tends to follow the curve. It is also noted that the results of references 2 and 3 parallel these results down to a Bond number of about 9.

The immediate significance of the normalized damping coefficient is not in the inflections. What is important is the asymptotic behavior as the Bond number is decreased. The curve in figure 15 shows that the normalized damping coefficient tends to remain constant below Bond numbers of 100. The decrease in natural frequency compensates for the increase in the coefficient of the logarithmic decrement. These results imply that for identical radii and liquids the damping coefficient α is relatively independent of acceleration in the Bond number region from about 100 to 0.

The time required to damp a slosh wave to a fraction A of its amplitude is

$$T = \frac{\ln\left(\frac{1}{A}\right)}{\alpha} \tag{17}$$

(Exponential damping is assumed.) According to the preceding results for α, T will be nearly constant for Bond numbers from 0 to 100 for otherwise equal variables. The time required to reach a given residual free slosh wave amplitude is practically independent of acceleration in the Bond number region from about 100 to 0.

Dynamic Contact-Angle Effects

As was mentioned previously, the static contact angle θ_s was near 0^o for all systems tested. The value of the static contact angle is important because of its dominating effect on both the low Bond number interface shape and the low Bond number sloshing frequency. Of equal importance is the possible dynamic variation of the contact angle during the sloshing motion. If the contact angle changes during sloshing, it is known that the frequency and damping (refs. 1 and 7) will be affected.

In this study, parameters were chosen to presume a near 0^o contact angle. No measurable change in the contact angle was observed for the data presented. A visual check is sufficient to detect gross contact-angle changes. However, minor variations in the contact angle usually cannot be measured because of refraction near the wall of the cylinder. An estimate of the possible change in contact angle due to the sloshing motion was calculated. Unpublished NASA data confirm that the dynamic contact angle as given by Fritz (ref. 11) can be predicted by

$$\tan \theta_d = K\left(\frac{V\eta}{\sigma}\right)^{1/3} \tag{18}$$

The equation is rigorously applicable only for a steady interface velocity V and when the interface moves over a previously wetted liquid layer. The latter condition was observed in the fundamental mode.

Using the maximum instantaneous velocity of the slosh wave $A_n\omega_1$, equation (18) was used to calculate dynamic contact angles. While some values were as high as 25^o, the majority were less than 10^o. An examination of the data showed no systematic trend with these values. For example, the spread in the damping data of figure 13 could not be correlated with the estimated departure from a 0^o-contact-angle condition. Also, the behavior of the coefficient of the logarithmic decrement cannot be attributed to contact-angle variation. Based on these comparisons and the fact that the use of the maximum interface velocity greatly overestimates the probable dynamic effects, we concluded that variations in the contact angle for the data presented are entirely negligible.

SUMMARY OF RESULTS

An experimental investigation was conducted to determine the natural frequency and damping characteristics of small-amplitude lateral sloshing in low Bond number environments. The study employed right-circular cylinders, 0.317 to 3.17 centimeters in radius R, with hemispherical bottoms. Test liquids were restricted to those which pos-

sess near 0^{o} static contact angles on the cylinders' surfaces; effects due to dynamic variations in the contact angle were negligible. These liquids had viscosities η between 0.32 and 2.9 centipoise, surface tensions σ between 13.2 and 26.9 dynes per centimeter, and densities ρ between 0.79 and 1.72 grams per cubic centimeter. Experiments were conducted in both a normal-gravity environment and low-gravity environments ranging as low as 10^{-5} g. Data were obtained on the fundamental sloshing frequency and damping at Bond numbers Bo ranging from 0 (i.e., $\approx$0.001) to greater than 800. The study yielded the following results:

1. The change in the fundamental slosh-mode shape corresponded to the change in the equilibrium liquid surface shape with Bond number. Free lateral sloshing was observed to occur on a residual layer of liquid deposited by the initial slosh wave.

2. The natural frequency ω_1 at deep liquid depths (i.e., $h/R > 2$, where h is the liquid centerline depth) was empirically determined to follow the relation

$$\omega_1^2 = (2.6 + 1.84\ \mathrm{Bo})\frac{\sigma}{\rho R^3}$$

The relation confirms the zero Bond number result of reference 4 and reduces to the well known high Bond number limit.

3. The natural frequency data in hemispherical-bottom cylinders at shallow liquid depths (i.e., $h < 2R$) compared favorably with the analytical predictions of Concus, Crane, and Satterlee (ref. 6) at low Bond numbers and with the results of Budiansky and Riley (refs. 8 and 9) at high Bond numbers.

4. The damping in terms of the logarithmic decrement was determined to follow the relation

$$\delta = K_d\left(\frac{\eta}{\rho\omega_1 R^2}\right)^{1/2}$$

where the nondimensional damping constant K_d is a function of Bond number. At Bond numbers less than approximately 1, K_d had a value of 28.1, which is the zero Bond number damping constant. The value of K_d decreased rapidly in the Bond number region from approximately 1 to 100. Above Bond numbers of 100, K_d approached the value of 6.1 which is the established high Bond number damping constant.

5. The damping coefficient α can be predicted by using the correlations for δ and ω_1. The damping coefficient does not vary significantly from the zero Bond number value in the Bond number region from 0 to 100. In this region, the damping coefficient

is practically independent of the magnitude of the system acceleration for otherwise equal cylinder radii and liquid properties.

Lewis Research Center,
National Aeronautics and Space Administration,
Cleveland, Ohio, November 12, 1968,
124-09-17-01-22.

REFERENCES

1. Abramson, H. Norman: The Dynamic Behavior of Liquids in Moving Containers, With Applications to Space Vehicle Technology. NASA SP-106, 1966.
2. Clark, Leonard V.; and Stephens, David G.: Simulation and Scaling of Low-Gravity Slosh Frequencies and Damping. 2nd ASTM, IES and AIAA Space Simulation Conference. ASTM, 1967, pp. 43-49.
3. Dodge, Franklin T.; and Garza, Luis R.: Simulated Low-Gravity Sloshing in Cylindrical Tanks Including Effects of Damping and Small Liquid Depth. Tech. Rep. 5, Southwest Research Inst. (NASA CR-61469), Dec. 29, 1967.
4. Salzman, Jack A.; Labus, Thomas L.; and Masica, William J.: An Experimental Investigation of the Frequency and Viscous Damping of Liquids During Weightlessness. NASA TN D-4132, 1967.
5. Salzman, Jack A.; Coney, Thom A.; and Masica, William J.: Effects of Liquid Depth on Lateral Sloshing Under Weightless Conditions. NASA TN D-4458, 1968.
6. Concus, P.; Crane, G. E.; and Satterlee, H. M.: Small Amplitude Lateral Sloshing in a Cylindrical Tank with a Hemispherical Bottom Under Low Gravitational Conditions. Rep. LMSC/A852007, Lockheed Missiles and Space Co. (NASA CR-54700), Jan. 20, 1967.
7. Miles, J. W.: Surface-Wave Damping in Closed Basins. Proc. Roy. Soc., Ser. A, vol. 297, no. 1451, Mar. 21, 1967, pp. 459-475.
8. Budiansky, Bernard: Sloshing of Liquids in Circular Canals and Spherical Tanks. J. Aero/Space Sci., vol. 27, no. 3, Mar. 1960, pp. 161-173.
9. Riley, James D.; and Trembath, Nat. W.: Sloshing of Liquids in Spherical Tanks. J. Aerospace Sci., vol. 28, no. 3, Mar. 1961, pp. 245-246.

10. Stephens, David G.; Leonard, H. Wayne; and Perry, Tom W., Jr.: Investigation of the Damping of Liquids in Right-Circular Cylindrical Tanks, Including the Effects of a Time-Variant Liquid Depth. NASA TN D-1367, 1962.

11. Friz, G.: On the Dynamic Contact Angle in the Case of Complete Wetting. Z. Angew. Phys., vol. 19, no. 4, July 1965, pp. 374-378.